EFFECT OF SPECIMEN GEOMETRY ON J_{Ic}, J_i AND THE J_R-CURVE

D.-Z. Sun*, D. Dormagen** and W. Dahl***

The effect of specimen geometry on J_{Ic}, J_i and the J_R-curve is investigated for Fe 510 and 42 CrMo 4 steel. The ASTM-procedure is compared with DCPD- and SZW-measurements. A procedure for an alternative technical initiation value $J_{0.2}$ is proposed showing less geometry dependences and approaching physical initiation values. The comparison between the calculated and experimentally determined blunting behaviour is presented. Geometry effects are discussed by 'J-controlled' crack growth conditions and differences in the state of stress and the influence of resistance behaviour on the instability of structural component is presented.

INTRODUCTION

The onset of stable crack growth is characterized by the technical initiation J_{Ic}-value according to ASTM E 813 /1/, or by physical initiation J_i-values using additional test techniques such as direct current potential drop (DCPD) /2,3/ or stretch-zone width (SZW) measurements /4,5/. Beyond initiation the material's crack growth behaviour is described by the J_R-curve. For the appropiate application of these values for a quantitative safety analysis of a structural component the geometry independence has to be assured. The conditions to be met for obtaining results under plane strain conditions are summarized in the American standard and confirmed on few materials, but also contradictory investigations have been reported /6-8/. These differences can be

* On leave from Beijing University of Iron and Steel Technology, Beijing, China
** Hoesch-Stahl AG, Dortmund, W.-Germany
*** Institute for Ferrous Metallurgy of the techn. University Aachen, W.-Germany

explained by inhomogeneous plate properties but also by different distances of the test temperature to the ductile/brittle transition of the material.

In this investigation a homogeneous plate of the low strength structural steel Fe 510 was used to evaluate the effect of specimen geometry on J_{Ic}, J_i and the J_R-curve. These results are compared with a high strength quenched and tempered 42 CrMo 4 steel. Besides the multi-specimen technique additional methods like direct current potential drop (DCPD)- and SZW-measurements were used to determine possible weak points of the ASTM-Standard E 813, being discussed in several national working groups resulting already in alternative proposals.

MATERIAL AND SPECIMEN GEOMETRY

The tests were carried out on 80 mm thick plates of the normalized Fe 510 steel and the steel 42 CrMo 4 in a quenched and tempered condition (840°C/water + 640°C/air). The chemical composition and the mechanical properties of tensile and charpy impact tests are listed in Tab. 1 for both steels. The structural steel shows homogenity across the plate thickness whereas only a 50 mm thick range in the mid-thickness position was appropriate for these investigations for the 42 CrMo 4 steel. This result was also affirmed by hardness measurements. The microstructure (see Fig. 1) shows bands of ferrite and pearlite with a mean ferrite grain diameter of d_m = 18 µm for the steel Fe 510 and a tempered bainite for 42 CrMo 4.

According to the ASTM procedure twelve geometry series for the structural steel and three series for the quenched and tempered steel were tested, varying the specimen thickness between 13 and 75 mm and the width between 26 and 150 mm, as shown in Tab. 2. Plane-sided and 20% side-grooved CT-specimens were prefatigued to an a/W-ratio of 0.6. Thus the effects of thickness, width, overall-dimensions and side-grooving could be evaluated separately. The tests were carried out in the upper shelf toughness regime at room-temperature. All specimens were tested in the T-L orientation.

EXPERIMENTAL PROCEDURE

The fracture mechanics tests were carried out in displacement control using servo-hydraulic testing machines (100 and 1000 kN) with a constant ram displacement speed of 0.4 mm/min.

Using the DCPD-method for crack initiation no characteristic change in the slope of the potential-displacement record was found for the very tough Fe 510 steel. In this case a multi-

specimen calibration technique as proposed by Bachmann /2,3/ was used to determine crack initiation by a back extrapolation of the potential change to stable crack extension $\Delta a = 0$. Thus plasticity effects were taken into account. For the less ductile quenched and tempered steel initiation could be determined by a significant change in slope. Both methods are demonstrated in Fig. 2a. The principle of SZW-measurements, carried out in a SEM, is shown in Fig. 2b. Because of the non-regular formation of the SZW a mean value of 70 equally spaced single values was determined for several specimens with and without side-grooves within the blunting-regime and for each serie one specimen was measured after crack initiation. The J_i-value was defined by an extrapolation against the measured blunting-line.

The J-integral was calculated after /1/ using

$$J = \eta \cdot \frac{A}{B(W-a_o)} \qquad (1)$$

RESULTS AND DISCUSSION

Determination of the blunting-line

The comparison between the calculated and experimentally determined blunting behaviour is demonstrated for both steels in Fig. 3. In Fig. 3a the ASTM-blunting line is compared with SZW-measurements and calculations from the 'HRR-field' /9/ using

$$J = \frac{\sigma_{ys} \cdot SZW}{d_n \cdot 0.4} \qquad (2)$$

both for plane strain and plane stress. The specimen size was 1TCT with 20% side-grooving. There is a good agreement between SZW-measurements and HRR-field calculations for plane strain. The slope for plane stress conditions is somewhat decreased, nevertheless measurements and theoretical considerations reveal that the generalized blunting procedure given by ASTM is overestimating the material's behaviour. A slope of 4.6 instead of 2 in

$$J = 2\sigma_y \cdot SZW \qquad (3)$$

was determined for this low strength, ductile structural steel.

For the high strength quenched and tempered steel 42 CrMo 4 (fig. 3b) there is a good agreement between SZW- measurements and HRR-field calculations for plane stress, both again demonstrating that the ASTM-procedure overestimates the material's blunting

behaviour. Compared to Fe 510 steel the differences between SZW-measurements/'HRR'-field calculations and the ASTM-blunting procedure seem to diminish with increasing yield strength.

Effect of specimen geometry on J_{Ic} and J_i

The effect of specimen geometry on crack initiation values is demonstrated in Fig. 4, where the ASTM-procedure is compared with DCPD- and SZW-measurements. Except for the 13 mm thick specimens the ASTM criteria

$$B, (W-a) > 15\ J/\sigma_y \tag{4}$$

and

$$B, (W-a) > 25\ J_{Ic}/\sigma_y \tag{5}$$

concerning geometry independence and plane strain conditions are met. Nevertheless J_{Ic}-initiation values are remarkably effected by the specimen geometry. J_{Ic}-values decrease about 17% with increasing thickness from 25 to 50 mm keeping the width constant. The same influence is observed, when the overall dimension are enlarged from 1TCT - to 3TCT specimens. Increasing the specimen width from 50 mm to 150 mm results in an increase of J_{Ic}-values of about 30%. This effect was found to be more pronounced with decreasing thickness /10/. Introducing 20%-side grooving generally lower J_{Ic}-values are determined although the slope of the J_R-curve (dJ/da) is equal for plane sided and side-grooved specimens, and is not effected by the overall dimensions. One has to notice that only above a thickness of B = 50 mm a geometry independent J_{Ic}-value was determined resulting in a geometry criterion:

$$B, (W-a) > 120\ J_{Ic}/\sigma_y \tag{6}$$

Comparing J_{Ic}-values with DCPD- and SZW-measurements one can see that significantly lower initiation values are determined with the latter methods. Both techniques result in similar J_i-values indicating that physical initiation can be detected rather by DCPD- and SZW-measurements. The experiments on the high strength steel 42 CrMo 4 revealed no significant geometry effects on J_{Ic}- or J_i-values. For all series the geometry criteria given by Eqs. (4) and (5) are met. DCPD-measurements again result in lower initiation values.
The geometry effects on J_{Ic}-values can be explained for steel Fe 510 as follows:

a) the ASTM blunting-line with $J = 2\ \sigma_y \cdot \Delta a$ overestimates the crack tip blunting especially for low strength high toughness steels. SZW-measurements have demonstrated the blunting-line to be better described by $J = 4.6\ \sigma_y \cdot \Delta a$, which was also demonstrated by HRR-field calculations

b) the ASTM-procedure refers to the J_R-curve but the conditions of 'J-controlled' crack growth are not applied sufficiently strict. Especially the geometry criterion $B > 25\ J_{Ic}/\sigma_y$ is not confirmed. These investigations propose a factor of 120 instead of 25. Theoretical investigations of Riedel /11/ propose a factor of at least 67, which is confirmed by using the ASTM procedure but considering the measured blunting-line in this investigation.
c) Combining these effects, the technical J_{Ic}-value can be determined in a region where stable crack growth has already occured, and where geometry dependent J_R-curves can be derived.

For steel 42 CrMo 4 no geometry effects (see Fig. 5) were measured in the range of specimen sizes investigated. At least a factor of 60 can be affirmed for geometry independence by the smallest specimen (1/2 T CT).

These investigations led to a proposal to determine a technical J-value for initiation suggested by Dahl et al. /10/, where based upon a power law fit of the J_R-curve initiation was defined at a constant value of $\Delta a = 0.2$ mm. These $J_{0.2}$-values are nearer to the physical initiation and demonstrate less pronounced geometry effects as shown in Fig. 4 for those series, where the effect of overall specimen dimensions was investigated.

The effect of geometry on the J_R-curve

In Fig. 6-8 the effect of geometry on the J_R-curve is shown for Fe 510 steel for plane sided and side-grooved specimens with variation of overall-dimension and for specimens with thicknesses B > 50 mm. The arrows in Fig. 6 and 7 characterize the limits of 'J-controlled' crack growth given by

$$\Delta a_{max} < 0.06b \tag{7}$$

$$b,B \geq 25\ J/\sigma_{ys} \tag{8}$$

$$\omega = \frac{dJ}{da} \cdot \frac{b}{J} > 10 \tag{9}$$

The J_R-curves are described by a power law fit given by

$$J = C_1 \cdot \Delta a^{C_2} \tag{10}$$

which seems to be more realistic than a linear regression especially in the regime of the onset of stable crack growth. For both series lower and flatter J_R-curves are measured with increasing overall dimensions. J_R-curves derived from side-grooved

specimens are lower than for plane sided specimens, but for both series geometry independence is indicated for a specimen thickness B ≧ 50 mm. This is also indicated in Fig. 8 where J_R-curves do not exhibit an influence of specimen width for B > 50 mm.

The conditions of 'J-controlled' crack growth given by Eqs. (7)-(9) are summarized in Tab. 3 for side-grooved and plane-sided specimens. For smaller specimens the thickness criterion (Eq. 8) to ensure plane strain behaviour is more severe and for larger specimens the maximum allowable crack extension and the ω-criterion to ensure proportional plastic deformation. The fact that within the thickness limits (Eq. (8)) but outside the Δa_{max}- and ω-criterion the J_R-curves are still geometry independent demonstrates that further experiments and theoretical work is necessary to determine the limits for the slope of the J_R-curve and the maximum allowable crack growth.
The differences in the crack resistance behaviour can be explained by different stress states ahead of the crack tip. The normalized load-displacement records in Fig. 9, describing the stress intensification ahead of the crack tip /12/, demonstrate for Fe 510 steel by the arrows characterizing the onset of stable crack extension that crack initiation appears for larger specimens at smaller displacement values. From that one can conclude that the behaviour of larger specimens is governed by a higher constraint.

The influence of the above mentioned geometry effects on the failure analysis of three different structural components is demonstrated in Fig. 10. Based on the Shih and Kumar concept /13/ the normalized J_{appl}-curves for the CCP, DECP and a cylindric specimen are compared with instability loads for the analysis carried out with the steepest and the flattest J_R-curve of 1TCT-13 and 2TCT-20% SG geometry. It is demonstrated that in the fully ductile regime (steep increase of J_{appl}) the remarkable geometry effect on the load bearing compacity is very small e.g. $\Delta (P/P_o)_{CCP} \cong 10\%$. It has to be emphasized that this geometry effect may be more pronounced for the amount of crack extension at instability loads.

CONCLUSIONS

The investigations revealed a strong influence of the specimen geometry on J_{IC}, J_i and J_R-curves especially when the conditions of 'J-controlled' crack growth are not met. The physical initiation values J_i determined by SZW- and DCPD measurements are generally lower than the technical J_{IC}-measurements and show geometry independence. This was explained by the overestimation of the blunting-line given by the ASTM procedure, thus technical values are determined in a regime of stable crack growth where J_R-curves are not geometry independent because the 'J-controlled'

crack growth conditions are not applied sufficiently strict in the ASTM standard. The thickness criteria $B > 25\ J_{Ic}/\sigma_y$ is not confirmed for a low strength structural steel. For steel Fe 510 a value of 120 and for 42 CrMo 4 a factor of 60 is necessary to ensure geometry independence. An alternative procedure for the determination of a technical $J_{0,2}$-value was proposed, being nearer to physical initiation values and showing less geometry dependence. The influence of the specimen geometry on the J_R-curve was explained by different stress states. For thicker, larger and side-grooved specimens plane strain conditions are approached. The influence of J_R-curve behaviour on the failure analysis of CCP-, DECP- and cylindrical specimens was discussed.

SYMBOLS USED

a_o = fatigue crack length
A = area under the load displacement record
b = ligament
B = thickness
C1, C2 = constants of power law, Eq (10)
CCP = center-cracked plate in tension
DCPD = direct current potential drop
DECP = double-edge cracked plate in tension
d_n = factor correlating J and COD, d_n = f (N, σ_{ys}, stress state) /14/
J = J-integral
J_i = J-integral at crack initiation from DCPD- or SZW-measurements
J_{Ic} = J-integral at crack initiation after ASTM E 813
$J_{0,2}$ = J-integral at a constant value of Δa = 0.2 mm /10/
N = strain-hardening exponent
P = load
P_o = limit load
SZW = stretch zone width
W = width
σ_y = average of the yield stress and the tensile strength
σ_{ys} = yield stress
η = factor, depending on the a/w-ratio

REFERENCES

/1/ ASTM E 813, Annual Book of ASTM Standards, Part 10 American Society of Testing and Materials, Philadelphia Pa, 1981

/2/ Bachmann, V.; Keller, H.P.; Munz, D.: Arch. Eisenhüttenwes. 55 (1984), No. 1, p. 33/40

/3/ Bachmann, V.: In Vorträge der 16. Sitzung des Arbeitskreises Bruchvorgänge, Deutscher Verband für Materialprüfung e.V., 21./22. Feb. 1984, Universität Karlsruhe, p. 201/12

/4/ Kobayashi, H.; Nakamura, H.; Nakazawa, H.: In: Elastic-Plastic Fracture, Second Symposium, Vol. II Philadelphia 1983. (ASTM Spec. Tech. Publ. No. 803) p. 420/28

/5/ Ohji, K.; Otsuka, A. and Kobayashi, H.: see 4) p. 398/419

/6/ Davis, D.A.; Vassilaros, M.G.; Gudas, J.P.: see 4) p. 582/610

/7/ Marandet, B.; Phelippeau, G.; De Roo, P.; Rousselier, G.: Institut De Recherches De la Siderurgie Francaise, Report 909, July 1982

/8/ Gibson, G.P.; Druce, S.G.: Metallurgy Division AERE Harwell, Report 10906, April 1983

/9/ Cornec, A.: Vorträge der 17. Sitzung des Arbeitskreises Bruchvorgänge, Deutscher Verband für Materialprüfung e.V., 12./13. Feb. 1985, in Basel, p. 417/25

/10/ Sun, D.-Z.; Dormagen, D.; Dahl, W.: Steel Research 56 (1985) No.8, p. 445/49

/11/ Riedel, H.: Vorträge der 16. Sitzung des Arbeitskreises Bruchvorgänge, Deutscher Verband für Materialprüfung e.V., 21./22. Feb. 1984, Universität Karlsruhe, p. 7/14

/12/ Andrews, W.R.; Shih, C.F.: In: Elastic-Plastic Fracture, Philadelphia 1979 (ASTM Spec. Tech. Publ. No. 668) p. 426/50

/13/ Kumar, V.; German, M.D.; Shih, C.F.: An Engineering Approach for Elastic-Plastic Fracture Analysis, NP-193/EPRI (1981)

/14/ Shih, C.F.: J. Mech. Phys. Solids 29 (1981) No. 4, p. 305/26

Chemical composition

Element	C	Si	Mn	P	S	Al	Cu	Cr	Ni	Mo
Fe 510	0,15	0,28	1,39	0,021	0,019	0,032	0,03	0,032	0,016	—
42CrMo4	0,41	0,24	0,59	0,017	0,020	—	—	0,92	—	0,22

Mechanical properties: Mid-thickness

	Tensile test				Charpy impact test	
	σ_{YS} N/mm²	σ_{UTS} N/mm²	ε_f %	RA %	CVN USE J	$T_{0.5}$ CVN USE K
Fe 510	317	489	27	68	86	253
42CrMo4	746	903	17	54	70	283

Tab. 1: Chemical composition and mechanical properties of Fe 510 and 42 CrMo 4 steel

Geometry series:
0% SG 20% SG
Fe 510 ○ ●
42 CrMo 4 □

Specimen thickness B [mm]	Specimen width W [mm] 26	50	100	150
13	○ ● □	○ □		
25		○ ● □	○	○
50		○	○ ●	
75				○ ●

Tab. 2: Specimen dimensions

Geometry Steel: Fe 510	J-integral [kJ/m²] $\Delta a \leq 0.06 b$	$b, B \geq 25 \frac{J}{\sigma_y}$	$\omega = \frac{dJ}{da} \frac{b}{J} > 10$
B13 W 26	265	133	231
B25 W 50	331	254	307
B50 W100	371	476	314
B75 W150	396	733	329
B13 W 26 20% SG	222	127	175
B25 W 50 20% SG	273	232	224
B50 W100 20% SG	298	449	252
B75 W150 20% SG	382	725	336

Tab. 3: Limit values of 'J-controlled' crack growth given by Eqs. (7)-(9)

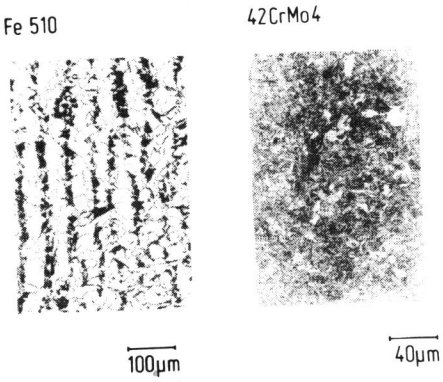

Fig. 1: Microstructure of Fe 510 and 42 CrMo 4 steel

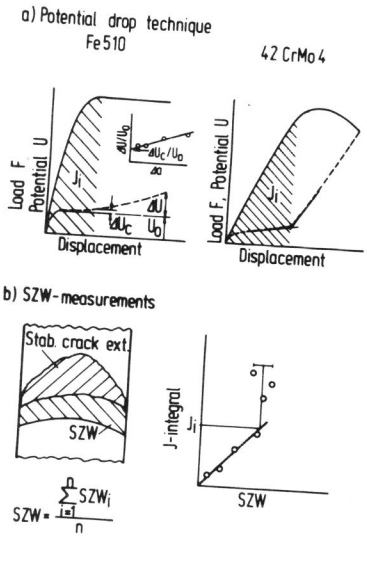

Fig. 2: Evaluation of crack initiation values a) with the DCPD-method, b) with SZW-measurements

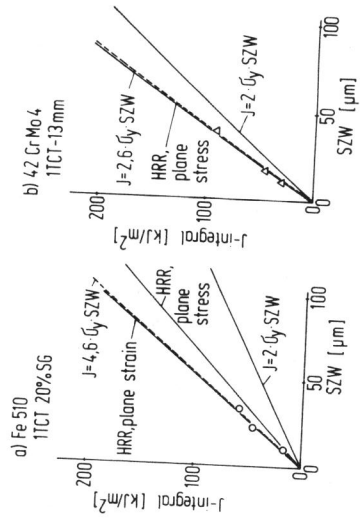

Fig. 3: Comparison between the calculated and experimentally determined blunting behaviour a) for Fe 510 and b) for 42 CrMo 4

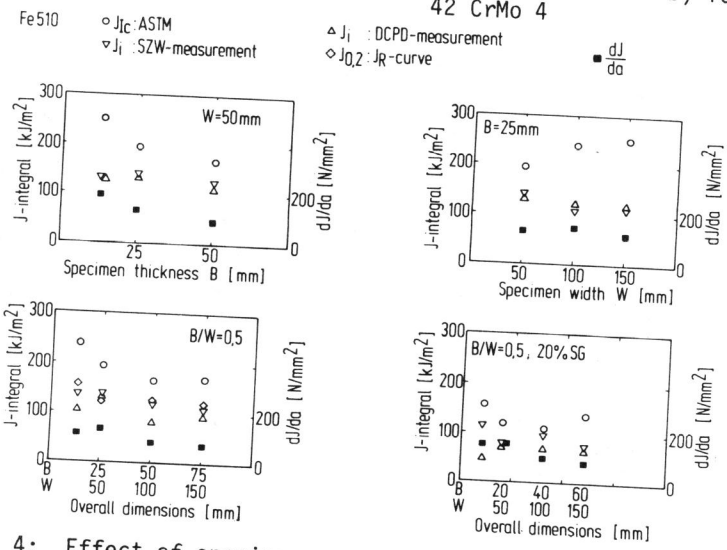

Fig. 4: Effect of specimen geometry on crack initiation values for Fe 510 steel

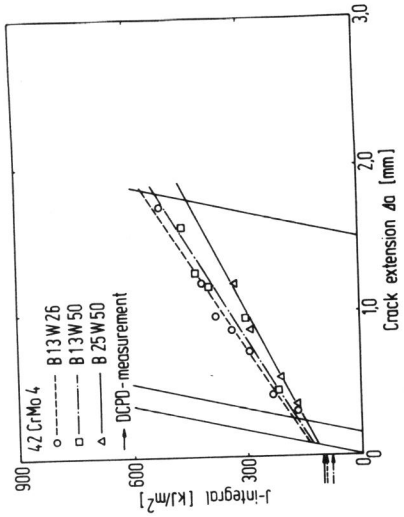

Fig. 5: Effect of specimen geometry on crack initiation values for 42 CrMo 4

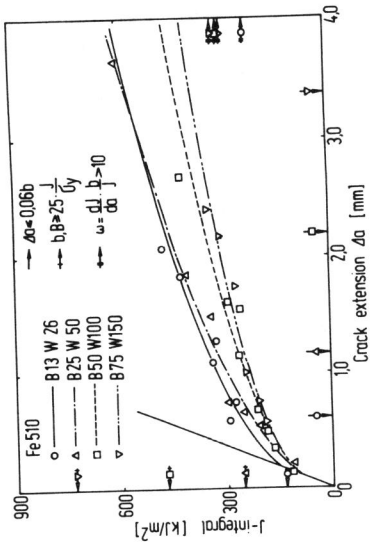

Fig. 6: Effect of overall specimen dimensions on J_R-curve of steel Fe 510

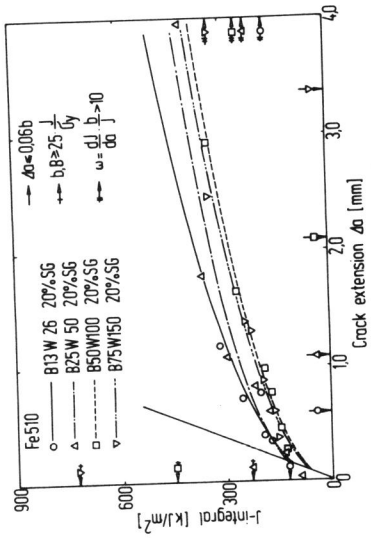

Fig. 7: Effect of 20% side-grooving on J_R-curve of steel Fe 510

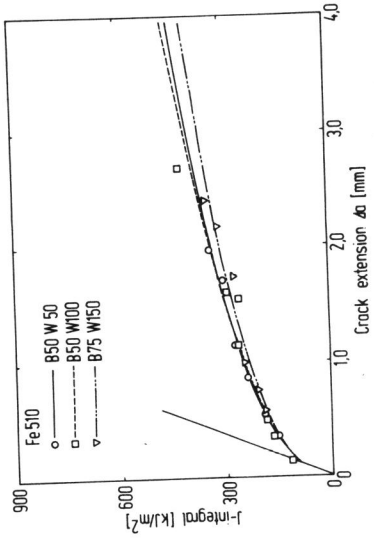

Fig. 8: Effect of specimen width for B ≥ 50 mm of steel 510

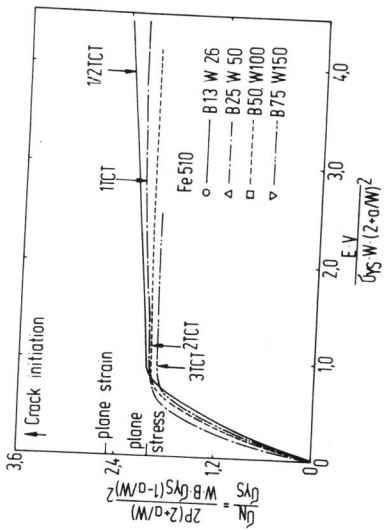

Fig. 9: Normalized load-displacement records for Fe 510 steel

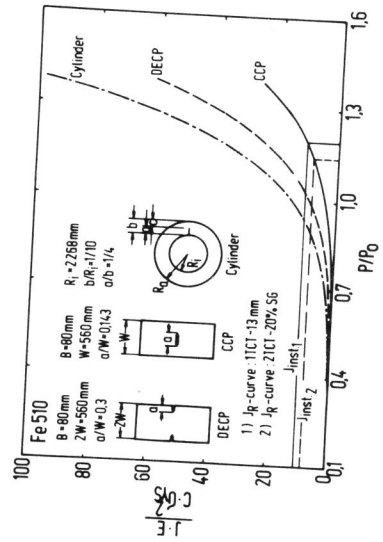

Fig. 10: Failure analysis of three different structural components for steel Fe 510